



**HAL**  
open science

# Establishment and Application of an Interplanetary Disturbance Index Based on the Solar Wind–Magnetosphere Energy Coupling Function and the Spectral Whitening Method

Xiaowei Zhao, Jingsong Wang, Mingxian Zhao, Ying D. Liu, Huidong Hu, Mingzhe Liu, Tian Mao, Qiugang Zong

► **To cite this version:**

Xiaowei Zhao, Jingsong Wang, Mingxian Zhao, Ying D. Liu, Huidong Hu, et al.. Establishment and Application of an Interplanetary Disturbance Index Based on the Solar Wind–Magnetosphere Energy Coupling Function and the Spectral Whitening Method. *The Astrophysical Journal*, 2024, 970, 10.3847/1538-4357/ad5000 . insu-04853428

**HAL Id: insu-04853428**

**<https://insu.hal.science/insu-04853428v1>**

Submitted on 23 Dec 2024

**HAL** is a multi-disciplinary open access archive for the deposit and dissemination of scientific research documents, whether they are published or not. The documents may come from teaching and research institutions in France or abroad, or from public or private research centers.

L'archive ouverte pluridisciplinaire **HAL**, est destinée au dépôt et à la diffusion de documents scientifiques de niveau recherche, publiés ou non, émanant des établissements d'enseignement et de recherche français ou étrangers, des laboratoires publics ou privés.



Distributed under a Creative Commons Attribution 4.0 International License



# Establishment and Application of an Interplanetary Disturbance Index Based on the Solar Wind–Magnetosphere Energy Coupling Function and the Spectral Whitening Method

Xiaowei Zhao<sup>1,2,3</sup> , Jingsong Wang<sup>2,3</sup> , Mingxian Zhao<sup>2,3</sup> , Ying D. Liu<sup>4,5</sup> , Huidong Hu<sup>4</sup> , Mingzhe Liu<sup>6</sup> ,  
Tian Mao<sup>2,3</sup> , and Qiugang Zong<sup>1</sup>

<sup>1</sup> School of Earth and Space Sciences, Peking University, Beijing 100871, People's Republic of China

<sup>2</sup> Key Laboratory of Space Weather, National Satellite Meteorological Center (National Center for Space Weather), China Meteorological Administration, Beijing 100081, People's Republic of China; [wangjs@cma.gov.cn](mailto:wangjs@cma.gov.cn)

<sup>3</sup> Innovation Center for FengYun Meteorological Satellite (FYSIC), Beijing 100081, People's Republic of China

<sup>4</sup> State Key Laboratory of Space Weather, National Space Science Center, Chinese Academy of Sciences, Beijing 100190, People's Republic of China

<sup>5</sup> University of Chinese Academy of Sciences, Beijing 100049, People's Republic of China

<sup>6</sup> LESIA, Observatoire de Paris, Université PSL, CNRS, Sorbonne Université, Université de Paris, 5 place Jules Janssen, 92195 Meudon, France

Received 2023 November 12; revised 2024 May 10; accepted 2024 May 17; published 2024 July 25

## Abstract

We develop a preliminary interplanetary disturbance index ( $J_s^W$ ) by applying the spectral whitening method to an energy coupling function with solar wind measurements during the years 1998–2014 as the input, which can be used as an indicator of perturbations in the near-Earth solar wind. The correlation and temporal variation between  $J_s^W$  and the geomagnetic disturbance index ( $J_p^G$ ) constructed from the same method have been analyzed in detail for 167 geomagnetic storms with the minimum  $D_{st}$  index less than or equal to  $-50$  nT. The time delay between  $J_s^W$  and  $J_p^G$  is clearly observable and varies for different events, according to which  $J_s^W$  is shifted backward with respect to  $J_p^G$ . We obtain a fairly good negative correlation between the shifted  $J_s^W$  and the  $J_p^G$  indices for the majority of events, and the significance level for 88% of the events (i.e., 147 events) does not exceed 0.05. A statistical analysis of the shifted  $J_s^W$  and the  $J_p^G$  indices for 147 selected events reveals that larger values of  $J_s^W$  and smaller magnitudes of  $J_p^G$  are commonly accompanied by enhanced southward magnetic fields, which implies that more solar wind energy is entering the magnetosphere and thus causing strong geomagnetic storms. Furthermore, a linear fit of the two indices suggests that the evolution of  $J_p^G$  can be predicted about 2 hr in advance based on  $J_s^W$ , indicating that  $J_s^W$  can provide early warnings of possible disturbances in the geomagnetic fields, which is crucial for space weather monitoring and operational forecasting.

*Unified Astronomy Thesaurus concepts:* Solar wind (1534); Interplanetary magnetic fields (824); Solar-terrestrial interactions (1473); Space weather (2037)

*Materials only available in the [online version of record](#): machine-readable table*

## 1. Introduction

Solar wind transient flows and the ubiquitous interplanetary magnetic fields (IMFs) are the primary sources of perturbations in the near-Earth space environment. Specifically, the prolonged southward components of the IMFs (negative  $B_z$ ) can reconnect with the front-side geomagnetic field, allowing more particles, momentum, and energy to enter the Earth. This can cause an enhanced westward ring current surrounding the Earth and trigger a geomagnetic storm (e.g., Dungey 1961; Gonzalez et al. 1994). Such storms are closely associated with various interplanetary drivings, such as interplanetary coronal mass ejections (ICMEs), corotating interaction regions (CIRs), and others (e.g., Gosling et al. 1991; Gonzalez et al. 1999; Zhang et al. 2007; Liu et al. 2014, 2020; Hu et al. 2016; Kilpua et al. 2017), and their intensities are generally quantified by the minimum value of the disturbance storm time ( $D_{st}$ ) index. There are plenty of indices in the solar–terrestrial space weather causal chain to symbolize the variations in solar activity,

geomagnetic effects, and ionospheric disturbances, respectively (e.g., Rostoker 1972; Mayaud 1980; Jakowski et al. 2006; Tapping 2013; Usoskin 2017, and references therein). However, no such index of measurements in interplanetary space seems to exist, although it is also important for understanding the impact of solar wind disturbances on the Earth's magnetosphere and ionosphere.

In the solar–terrestrial coupling system, our primary concern is with energy sources and sinks. By interacting with the magnetosphere, the solar wind transfers its energy into near-Earth space, and it is ultimately dissipated throughout the entire magnetosphere–ionosphere–thermosphere system (e.g., Akasofu 1981a; Lu et al. 1998; Østgaard et al. 2002; Turner et al. 2009). In particular, for episodic extreme events, the energy coupling there can create severe hazards for satellites, communications, power grids, and other infrastructure (e.g., Boteler et al. 1998; Pirjola et al. 2000; Oughton et al. 2017; Riley et al. 2018). Hence, quantifying how much solar wind energy is transferred to the magnetosphere is challenging for space weather monitoring. Over the past few decades, several coupling functions have been proposed from a qualitative or quantitative view (e.g., Kan & Lee 1979; Vasyliunas et al. 1982; Gonzalez 1990; Newell et al. 2007; Tenfjord & Østgaard 2013; Wang et al. 2014a;

McPherron et al. 2015, and references therein). Specifically, Perreault & Akasofu (1978) introduce an energy coupling function to estimate the input power of the solar wind energy to the magnetosphere. The function is

$$\varepsilon = \frac{4\pi}{\mu_0} VB^2 l_0^2 \sin^4\left(\frac{\theta}{2}\right) \quad [\text{W}], \quad (1)$$

where  $\mu_0$  is the permeability,  $V$  is the solar wind speed,  $B$  is the IMF's strength in the geocentric solar magnetic (GSM) coordinates,  $l_0$  is about 7 Earth radii, and  $\theta$  is the clock angle between the projection of the IMF in the  $y$ - $z$  plane and the  $B_z$  component. The  $\varepsilon$  parameter has been widely employed in studies characterizing its association with the storm intensity, the energy budget in the Earth's magnetosphere and ionosphere, and the development of geomagnetic storms (e.g., Akasofu 1981a, 1981b; Pulkkinen et al. 2002; Vichare et al. 2005; Zhang et al. 2008b; Turner et al. 2009; Guo et al. 2011; Li et al. 2012). Given its validity in describing the transfer of solar wind energy to the magnetosphere and its sensitivity to the southward transition of the IMF's  $B_z$  component, we utilize it as the preferred function to develop a preliminary interplanetary disturbance index in the present work.

Indices in different regions can be used to assess the chain impact of perturbations in solar-terrestrial space, which often exhibit delayed effects. The variations in geomagnetic fields associated with the solar cycle have been extensively studied in previous works, especially the analyses of correlation and time delay between the solar and geomagnetic indices (e.g., Cliver et al. 1996; Kishcha et al. 1999; Echer et al. 2004; Verbanac et al. 2010, 2011; Hajra et al. 2021). Echer et al. (2004) argue that the evolution of both the sunspot number and the 3 hr antipodal  $aa$  activity index vary in phase around 1868–1910, after which the correlation decreases, especially in solar cycle 22 where the  $aa$  index lags by two years due to its dual-peak structure. There are also many studies focused on how solar wind parameters relate to the geomagnetic indices (Meng et al. 1973; Gonzalez & Echer 2005; Maggiolo et al. 2017; Marques de Souza et al. 2018; Boroyev et al. 2020). Based on the solar wind measurements at IMP-8, Baker et al. (1981) indicate that both the dawn-dusk electric field and the  $\varepsilon$  parameter are about 40 minutes ahead of the auroral electrojet (AE) index. According to Gonzalez et al. (1989), the average time delays between various energy coupling functions and the  $D_{st}$  index for several intense geomagnetic storms are close to 1 hr. Therefore, the time delay is a crucial factor that cannot be ignored when exploring the correlations between indices in distinct regions.

Diverse periodicities ranging from a few days to decades are commonly seen in the solar and interplanetary parameters, geomagnetic activity indices, and the energy transferred into the magnetosphere (e.g., Mursula & Zieger 1996; Prabhakaran Nayar et al. 2002; Katsavrias et al. 2012; Andriyas & Andriyas 2017; Marques de Souza Franco et al. 2021), which are all modulated by the solar cycle (e.g., Hathaway 2015, and references therein). Additionally, for an arbitrary time series, the important factor is the perturbation, not the background, i.e., the periodic component or the noise. Wang et al. (2014b) propose the spectral whitening method (SWM) to extract aperiodic perturbations in the ionosphere, which has been demonstrated to be more sensitive to external geomagnetic effects than the often used monthly median method. They also

suggest that the standardized SWM-derived indices are comparable since the probability density functions are similar to a Gaussian distribution, which enables the development of a novel set of indices to monitor disturbances in solar-terrestrial space. By applying the SWM to the ionospheric F2-layer critical frequency (foF2) and the total electron content data, Chen et al. (2014, 2017) have established three ionospheric disturbance indices to depict aperiodic variations on single, planetary, and regional scales, which respond well to the  $D_{st}$  index. Zhao et al. (2022) further construct a new geomagnetic disturbance index ( $J_p^G$ ) with the same method based on the horizontal component of the geomagnetic field measured at eight ground-based observatories. In their study, the  $J_p^G$  index, with a temporal resolution of one hour, is capable of characterizing the changes in geomagnetic activity on a global scale, and its correlation with the  $D_{st}$  index has been rigorously verified. Given the usefulness of the SWM in developing indices describing the aperiodic changes in the geomagnetism and ionosphere, it is desirable to build a similar index in interplanetary space, with the goal of using the same set of indices to predict the chain impacts caused by transient flows on near-Earth space.

In this work, we establish a preliminary interplanetary disturbance index ( $J_s^W$ ) based on the SWM and the  $\varepsilon$  parameter, filling a gap in indices for monitoring solar wind perturbations in the near-Earth region. We illustrate how to determine its correlation and temporal variation with the geomagnetic disturbance index ( $J_p^G$ , see below) during the period of a mainly southward magnetic field component associated with geomagnetic storms. We also perform a statistical analysis to evaluate how and to what extent  $J_p^G$  is regulated by  $J_s^W$ , which is important for space weather forecasting. This paper is organized as follows. We introduce the data and methodology in Section 2. Event studies are provided in Section 3. Statistical analysis is presented in Section 4. The results are concluded and discussed in Section 5.

## 2. Data and Methodology

A primary purpose of this work is to introduce a new unique interplanetary disturbance index and to examine its usefulness in describing the development of the  $J_p^G$  index. In previous studies (Chen et al. 2014; Zhao et al. 2022), the ionospheric and geomagnetic disturbance indices are denoted as  $J_p$  and  $J_p^G$ , respectively, with the letter ‘‘p’’ indicating a ‘‘planetary scale’’ index constructed on the basis of observations from multiple ground-based stations distributed at low and middle latitudes, and ‘‘G’’ representing the geomagnetic field. In this paper, we use  $J_s^W$  to signify the interplanetary disturbance index, where the letter ‘‘s’’ shows an index established on the basis of single-point observations, and ‘‘W’’ denotes the solar wind. Hourly low-resolution solar wind plasma and magnetic field measurements from the OMNI data set during the period 1998–2014 have been utilized to compute the magnitude of the input power of solar wind energy to the magnetosphere (Perreault & Akasofu 1978; Koskinen & Tanskanen 2002, the  $\varepsilon$  parameter). Note that the IMFs are sampled in the GSM coordinates. The horizontal component of the geomagnetic field from INTERMAGNET is used to recalculate the  $J_p^G$  index (see below), and the time resolution is one hour. The adoption of low-temporal-resolution data in this work serves the purpose of aligning  $J_s^W$  and  $J_p^G$  and enabling them to be directly comparable. In future work, high-resolution data will be employed to further examine

**Table 1**  
List of Key Parameters of Geomagnetic Storms during 1998–2014

| #   | Date <sup>a</sup>       | $D_{st}$ <sup>a</sup><br>(nT) | Start <sup>b</sup><br>(UT) | End <sup>b</sup><br>(UT) | CC <sup>c</sup> | Delay <sup>d</sup><br>(hr) | CC <sup>e</sup> | $p$ -value <sup>f</sup> | $k$ <sup>g</sup> | $b$ <sup>g</sup> |
|-----|-------------------------|-------------------------------|----------------------------|--------------------------|-----------------|----------------------------|-----------------|-------------------------|------------------|------------------|
| 32  | 2000/07/16              | −300                          | 07/15 18:00                | 07/16 01:00              | −0.12           | 1                          | −0.84           | 0.009                   | −0.15            | −0.61            |
| 33  | 2000/07/20              | −92                           | 07/19 20:00                | 07/20 14:00              | −0.03           | 6                          | −0.78           | 0.000                   | −1.16            | −0.15            |
| 44  | 2001/03/31              | −387                          | 03/31 02:00                | 03/31 08:00              | −0.55           | 1                          | −0.96           | 0.000                   | −0.39            | 3.36             |
| 51  | 2001/09/13 <sup>h</sup> | −57                           | 09/13 01:00                | 09/13 07:00              | 0.34            | 3                          | −0.85           | 0.015                   | −1.85            | 0.20             |
| 82  | 2003/06/08 <sup>i</sup> | −50                           | 06/08 13:00                | 06/09 00:00              | −0.03           | 2                          | −0.61           | 0.033                   | −0.65            | −0.22            |
| 140 | 2012/02/19              | −63                           | 02/18 19:00                | 02/19 06:00              | −0.04           | 3                          | −0.92           | 0.000                   | −2.68            | 0.31             |
| 159 | 2013/10/02 <sup>j</sup> | −72                           | 10/02 03:00                | 10/02 07:00              | −0.20           | 2                          | −0.80           | 0.102                   | −0.74            | 0.16             |
| 160 | 2013/10/09              | −69                           | 10/08 17:00                | 10/09 08:00              | 0.37            | 3                          | −0.62           | 0.011                   | −1.05            | −0.11            |
| 161 | 2013/11/07              | −50                           | 11/07 00:00                | 11/07 12:00              | −0.13           | 2                          | −0.78           | 0.002                   | −1.43            | 0.07             |
| 162 | 2013/11/09              | −80                           | 11/08 23:00                | 11/09 12:00              | 0.16            | 4                          | −0.84           | 0.000                   | −0.98            | 0.08             |

#### Notes.

<sup>a</sup> The date and minimum value of the  $D_{st}$  index for each event.

<sup>b</sup> The start and end times cover the main southward component of the IMF.

<sup>c</sup> The correlation coefficient between  $J_s^W$  and  $J_p^G$  in the above time interval.

<sup>d</sup> The time delay yielded from a cross-correlation analysis of  $J_s^W$  and  $J_p^G$ .

<sup>e</sup> The correlation coefficient between the shifted  $J_s^W$  and the  $J_p^G$  indices.

<sup>f</sup> The significance level of the correlation coefficient between the shifted  $J_s^W$  and the  $J_p^G$  indices. Note that the  $p$ -value for each event is rounded to three decimal places, and a value of 0.000 is not a strict zero value but a value less than  $5.0 \times 10^{-4}$ .

<sup>g</sup> The  $k$  and  $b$  obtained from a linear fit of the shifted  $J_s^W$  and the  $J_p^G$  indices.

<sup>h</sup> A time delay greater than 0 has been chosen for these events since  $J_s^W$  is assumed to precede  $J_p^G$  by several hours.

<sup>i</sup> The time delay corresponding to the second minimum value of the cross-correlation coefficient is selected for this event due to the impact of the specified time interval.

<sup>j</sup> The significance level for these events is greater than 0.05, and they have all been excluded from the statistical analysis.

(This table is available in its entirety in machine-readable form in the [online article](#).)

the correlation between the two indices. We also exploit the  $D_{st}$  index from the World Data Center (WDC) for Geomagnetism in Kyoto to perform a survey of geomagnetic storms. The selection rules and associated methods are described below.

### 2.1. Selection Criteria for Geomagnetic Storms

The development of a typical geomagnetic storm is characterized by three phases: the initial, the main, and the recovery phases. Specifically, the main phase refers to a period from the initial decrease of the  $D_{st}$  index to its minimum, and then the slow recovery phase closely follows, during which the  $D_{st}$  index increases from its minimum to the pre-storm level. Sudden fluctuations in the solar wind, especially those in the southward magnetic field component, can significantly impact the morphology of the  $D_{st}$  index. In this work, we select geomagnetic storms with a “classic”  $D_{st}$  profile that exhibits only one temporary decrease (a single dip) in the main phase (e.g., Kamide et al. 1998; Zhang et al. 2008a). Events with multiple dips are not considered here as they are closely associated with the intermittent injection of energy into the magnetosphere (Akasofu 1980, 1981a, 1981b), which corresponds to a more complex solar wind–magnetosphere energy coupling process. A computer-based algorithm proposed by Zhang et al. (2008a) has been applied to identify geomagnetic storms with  $D_{st} \leq -50$  nT during the years 1998–2014. The three-hour smoothed  $D_{st}$  index and a threshold of about 14 nT, which is the standard deviation of  $D_{st} > -50$  nT, are used to distinguish the major dips, as suggested by Zhang et al. (2008a). We filter possible geomagnetic storms by visual inspection carefully, and we eventually select 167 qualified events (see Table 1). It should be noted that our focus in this work is on events with a single dip in the main phase of the  $D_{st}$

profile, therefore events with an additional, smaller dip in the recovery phase have not been excluded from the storm lists. For two or more adjacent occurring geomagnetic storms, we treat them as isolated events if they have almost recovered to pre-storm levels. Events with unavailable data or a short duration of the IMF’s southward component (less than 3 hr) are eliminated from this study.

### 2.2. Spectral Whitening Method

The SWM, proposed by Wang et al. (2014b), has been successfully applied to establish the ionospheric and geomagnetic disturbance indices (Chen et al. 2014, 2017; Zhao et al. 2022). The main spectral whitening process is formulated as follows:

$$g_d^*(t) = \int_{-\infty}^{+\infty} \left[ \int_{-\infty}^{+\infty} g(t) e^{-2\pi i t \xi} dt \right] \frac{P_0}{P_{env}(\xi)} e^{2\pi i t \xi} d\xi, \quad (2)$$

where  $g(t)$  is the original data time series,  $P_{env}(\xi)$  is the upper envelope of the power spectrum of  $g(t)$  estimated from its maximum value for a given window, and  $P_0$  is the mode of  $P_{env}(\xi)$ . According to Equation (2), the Fourier transform of  $g(t)$  is multiplied by a scaling factor, which can flatten the power spectrum and thus allow the identification of a perturbed component superimposed on  $g(t)$ .

In this work, we take the  $\varepsilon$  parameter as  $g(t)$  and extract its aperiodic component via Equation (2). To facilitate comparisons with other indices constructed using the same method, the derived result ( $g_d^*(t)$ ) is normalized by dividing it by its standard deviation. The final  $J_s^W$  index is a three-point running average of the normalized  $g_d^*(t)$ , as the whitening process may slightly enhance the noise during the squeezing of periodic

components. Similarly, we recalculate the geomagnetic disturbance index ( $J_p^G$ ) established by Zhao et al. (2022) on the basis of the SWM and the horizontal component of the geomagnetic field from eight ground-based stations (the specific locations of these stations are referred to in Figure 3 in their paper), which comprise the four sites used to measure the  $D_{st}$  index. The retrieval of aperiodic disturbances in the geomagnetic field at each station is consistent with that of the  $\varepsilon$  parameter, and the final  $J_p^G$  index is obtained by averaging the identified disturbances at the eight stations. If one wants to obtain a real-time index ( $J_s^W$ ,  $J_p^G$ , or others), it is necessary to accumulate measurements from satellite- or ground-based sources over multiple years or months, along with real-time observations, before the application of the SWM. Note that both  $J_s^W$  and  $J_p^G$  are dimensionless and developed in the same frame. This is useful for comparison and also for space weather forecasting.

### 2.3. Cross-correlation Analysis

Cross-correlation analysis has been extensively used in previous studies since it can determine the similarity between two different time series as well as the temporal displacement, i.e., the time delay (e.g., Meng et al. 1973; Baker et al. 1981; Verbanac et al. 2010, 2011; Marques de Souza et al. 2018; Hajra et al. 2021). In this work, we examine the association between  $J_s^W$  and  $J_p^G$  through a cross-correlation analysis for all events. Given that the occurrence of geomagnetic storms typically lags the injection of energy into the magnetosphere,  $J_s^W$  is assumed to precede  $J_p^G$  by a few hours. Thus, the time delay ( $\Delta t \geq 0$ ) corresponds to the time at which the peak value of the negative cross-correlation coefficient occurs. We shift  $J_s^W$  backward by  $\Delta t$  hours in order to align it with  $J_p^G$  and then apply a linear fit,

$$J_p^G(t) = k \times J_s^W(t - \Delta t) + b, \quad (3)$$

to quantify their relationship. The slope  $k$  indicates the average rate of change between the shifted  $J_s^W$  and the  $J_p^G$  indices, and the intercept  $b$  denotes the average variation of  $J_p^G$ .

Considering the crucial importance of the IMF's southward component in regulating the energy coupling mechanism associated with geomagnetic storms (e.g., Gonzalez & Tsurutani 1987; Gonzalez et al. 1989, 1994; Kamide 1992), we select a time interval bracketing the entire negative  $B_z$  component to perform the cross-correlation analysis and explore the association between  $J_s^W$  and  $J_p^G$ . For several events, the southward magnetic field component is occasionally interspersed with the northward one. We also calculate the time differences between the time when the minimum  $J_p^G$  is observed and the leading and trailing edges of the selected time interval. If both of them are less than 12 hr, we extend the longer of them to both ends with the minimum value of  $J_p^G$  as the midpoint, obtaining a new interval for the cross-correlation analysis, which can help reduce errors caused by using too short a time interval. The significance level of the correlation coefficient between the shifted  $J_s^W$  and  $J_p^G$  indices is assessed based on a  $p$ -value (e.g., Press et al. 1992, output by running the `corrcoef` function in MATLAB). If the  $p$ -value is 0.05 or below, then the two indices are considered to be significantly correlated in the present work.

## 3. Event Analysis

We make a survey of geomagnetic storms with the minimum  $D_{st} \leq -50$  nT during the period 1998–2014, which yields 167 “classic” events. The details of each event are listed in Table 1, including the date, the minimum value of the  $D_{st}$  index, the start and end times bracketing the main southward magnetic field component, the correlation coefficient between  $J_s^W$  and  $J_p^G$ , the time delay from the cross-correlation analysis, the correlation coefficient between the shifted  $J_s^W$  and the  $J_p^G$  indices, the  $p$ -value,  $k$ , and  $b$ . A first impression from Table 1 is that the correlation coefficient between the shifted  $J_s^W$  and the  $J_p^G$  indices is negative and clearly better than without the time delay, and the  $p$ -value for most events is no more than 0.05. This validates the linear quantitative relationship between the shifted  $J_s^W$  and the  $J_p^G$  indices (see Equation (3)). Furthermore, each of the 167 events has a unique  $k$  ranging from  $-2.68$  to  $-0.15$ , with a median value of  $-0.98$  and a standard deviation of 0.51, and its variation is primarily determined by the magnitudes of the two indices (and is possibly associated with the storm intensity), with only a minor contribution from the small statistics for each storm. Here we provide a detailed analysis of two examples, a strong geomagnetic storm and a moderate one, to illustrate how  $J_s^W$  is employed to estimate  $J_p^G$ . Also be aware that once the examination of the two indices on the space weather operational platform is completed, we will proceed to open-source them to the public.

### 3.1. The 2003 November 20 Geomagnetic Storm

On 2003 November 20, an intense geomagnetic storm occurred with a minimum  $D_{st}$  index of  $-422$  nT, which was caused by the prolonged and enhanced southward magnetic field carried by a magnetic cloud (Gopalswamy et al. 2005). Figure 1 (left) shows the 1 hr low-resolution magnetic field measurements from the OMNI database, along with the energy coupling parameter  $\varepsilon$ ,  $J_s^W$ ,  $J_p^G$ , and the  $D_{st}$  index. Obviously, the storm is related to the occurrence of the enhanced southward magnetic field in the shaded region. The absolute value of the minimum  $B_z$  component is almost equivalent to the magnetic field strength, about 51 nT and 56 nT, respectively. We notice that the development of the  $\varepsilon$  parameter corresponds well to the transition in the  $B_z$  component, and the extrema of both parameters coincide with each other. A few hours after the peak of the  $\varepsilon$  parameter, the minimum value of the  $D_{st}$  index is observed, and it is followed by a long period of recovery. The morphologies of the  $J_s^W$  index and the  $\varepsilon$  parameter present a high level of similarity, and the correlation coefficient between them is about 0.94 during November 20–22. It is crucial to emphasize that while the two parameters are strongly analogous, the  $J_s^W$  index is dimensionless and designed to capture and characterize the implicit disturbances within the  $\varepsilon$  parameter, allowing for a direct comparison with the  $J_p^G$  index. Moreover, the evolution of the  $J_p^G$  and  $D_{st}$  indices is also comparable with the minor distinction that the time it takes for  $J_p^G$  to reach its minimum and recover to a quiet level is shorter than that for the  $D_{st}$  index, as suggested by Zhao et al. (2022). The correlation coefficient between them during the entire time interval is 0.87, which highlights the practicality of  $J_p^G$ .

As mentioned earlier, we select the shaded region covering the prominent southward magnetic field component to examine the correlation and temporal variation between  $J_s^W$  and  $J_p^G$ . The two indices are almost not correlated with each other, with their

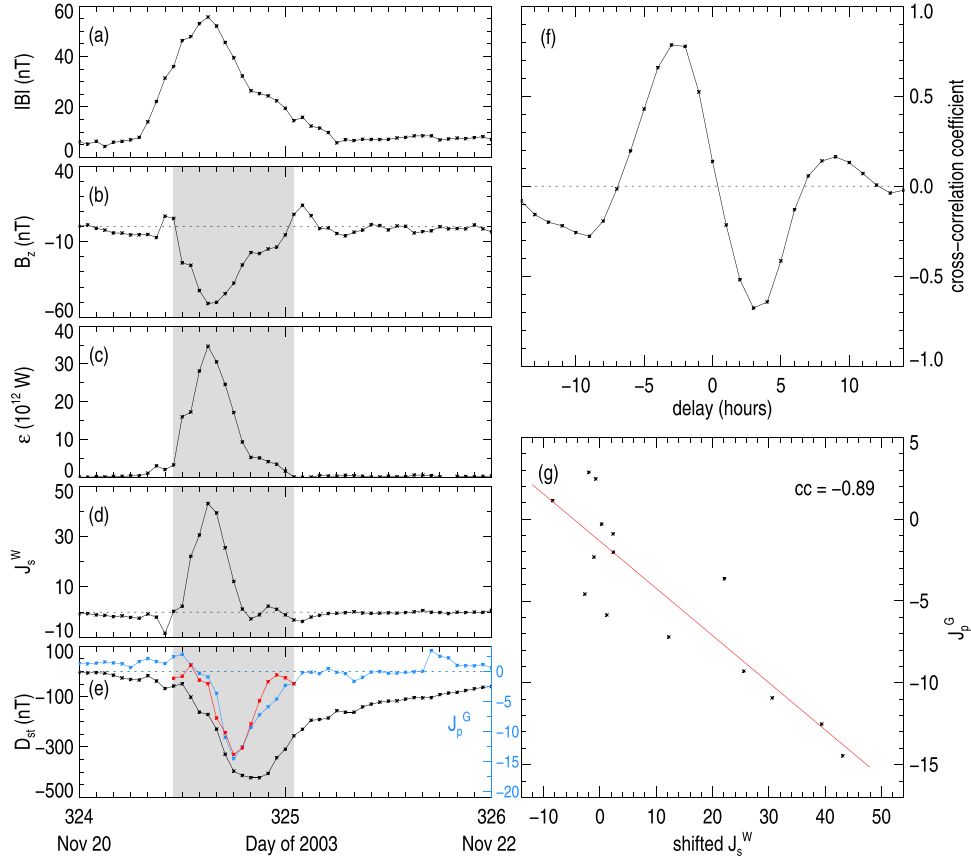


**Figure 1.** Left: key parameters associated with the geomagnetic storm that occurred on 2003 November 20. From top to bottom, the panels show the IMF’s strength, its north–south component, the  $\varepsilon$  parameter,  $J_s^W$ , and  $J_p^G$  (blue curve) superimposed on the  $D_{st}$  index (black curve). The shaded region indicates the time interval that encloses the main southward magnetic field component. Top right panel: cross-correlation analysis of  $J_s^W$  and  $J_p^G$  as a function of delay. Bottom right panel: correlation between the shifted  $J_s^W$  and the  $J_p^G$  indices. The red line indicates a linear fit of the two indices, and the deduced  $J_p^G$  index can be seen in the bottom panel on the left (the red curve).

correlation coefficient being only 0.14. Figure 1(f) displays the cross-correlation analysis of the two indices with a step of 1 hr. The  $J_s^W$  index is 3 hr ahead of the  $J_p^G$  index since the cross-correlation coefficient reaches its minimum value of about  $-0.68$  at this time. Hence, we shift  $J_s^W$  backward by 3 hr to align it with  $J_p^G$ , and the new correlation between the shifted  $J_s^W$  and the  $J_p^G$  indices is presented in Figure 1(g). One can easily see that the two indices are anticorrelated with a higher correlation coefficient of about  $-0.89$ , of which the significance level is smaller than  $5.0 \times 10^{-4}$ . We apply a linear fit of the shifted  $J_s^W$  and the  $J_p^G$  indices to quantify their relationship, which gives  $J_p^G(t) = -0.29 \times J_s^W(t - 3) - 1.35$ . The significant contrast in the magnitudes of the two indices, as shown in Figures 1(d) and (e), gives rise to a larger slope  $k$ . The smaller intercept  $b$  indicates that the average disturbance level of  $J_p^G$  is stronger during this intense storm. The modeled  $J_p^G$  index (red curve in Figure 1(e)) resembles the initial one (blue curve), in terms of not only the magnitude of decrease but also the time development. In other words, the evolution of  $J_p^G$  with a delay of several hours can be roughly described based on  $J_s^W$ , thus verifying the usefulness of  $J_s^W$  as an indicator of near-Earth solar wind perturbations. It is worth noting that lower values of the southward magnetic field component in the shaded region are accompanied by smaller or negative values of the shifted  $J_s^W$  index as well as larger or positive values of the  $J_p^G$  index,

implying that the geomagnetic field is at a stable level or the disturbance is relatively weak.

### 3.2. The 2004 February 11 Geomagnetic Storm

A moderate geomagnetic storm with a minimum  $D_{st}$  index of  $-93$  nT appeared on 2004 February 11 and was associated with a CIR (Jian et al. 2006; Zhang et al. 2007). Magnetic field measurements, as well as the  $\varepsilon$  parameter and other relevant indices, are shown in Figure 2 (left). The duration of the negative  $B_z$  component in the shaded region is 12 hr, with a minimum value of  $-14$  nT. Like the 2003 November 20 event, the  $\varepsilon$  parameter varies similarly as the  $B_z$  component rises and falls in the shaded region. The maximum magnitude of the  $\varepsilon$  parameter is observed at 15:00 UT on February 11 and is of the order of  $1.8 \times 10^{12}$  W, and two hours later the  $D_{st}$  index reaches its minimum value. Besides, there is a second sharp increase in the  $\varepsilon$  parameter during the storm’s recovery phase, despite the  $B_z$  component being smaller and fluctuating, resulting in another dip in the  $D_{st}$  index albeit weak. Note that the strength of the  $\varepsilon$  parameter (see Equation (1)) depends on not only the clock angle associated with the  $B_z$  component, but also the solar wind speed and the magnetic field strength. If their values are greater than 0, then the solar wind energy is transferred into the magnetosphere. During February 11–13, the development of  $J_s^W$  is roughly consistent with that of the  $\varepsilon$  parameter, and the same trend can also be seen in the evolution of the  $J_p^G$  and  $D_{st}$  indices, which

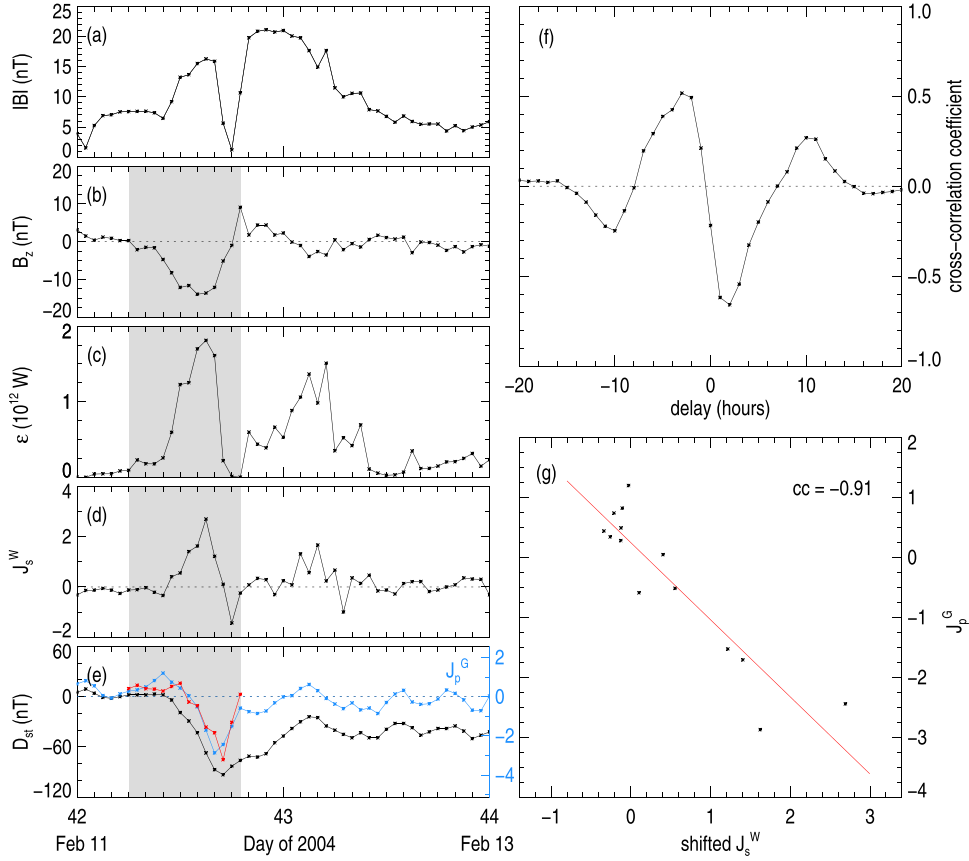


**Figure 2.** Similar to Figure 1, but for the geomagnetic storm that occurred on 2004 February 11.

verifies the usefulness of  $J_p^G$  again. Here, we re-emphasize that the dimensionless  $J_s^W$  index describes the perturbations that are concealed in the  $\varepsilon$  parameter, which is distinct from the original parameter itself.

The relationship between  $J_s^W$  and  $J_p^G$  in the shaded region is relatively weak with the correlation coefficient being only  $-0.28$ . Figure 2(f) presents analyses of the correlation and time delay of the two indices. The minimum value of the cross-correlation coefficient occurs at a time delay of 2 hr, which is equal to the time difference between the peaks of the  $\varepsilon$  parameter and the  $D_{st}$  index. Similarly, the  $J_s^W$  index is backward time-shifted by 2 hr with respect to  $J_p^G$ , and the resulting correlation is displayed in Figure 2(g). The correlation coefficient is considerably improved from  $-0.28$  to  $-0.91$ , with a significance level of less than  $5.0 \times 10^{-4}$ , highlighting the critical role played by the time delay in linking indices in various regions. The quantitative relationship acquired from a linear fit of the two indices,  $J_p^G(t) = -1.29 \times J_s^W(t - 2) + 0.25$ , is employed to predict  $J_p^G$ , which can be seen in Figure 2(e). The deduced and original  $J_p^G$  indices are analogous to each other, suggesting that  $J_s^W$  can serve as a reliable precursor for predicting geomagnetic storms. Furthermore, the weaker southward magnetic field components in the shaded region correspond to the minor magnitudes of the shifted  $J_s^W$  index and the higher values of  $J_p^G$ , both of which fluctuate around 0, as observed in the previous event.

#### 4. Statistical Analysis

We perform example analysis in Section 3 to validate the availability of  $J_s^W$  in depicting the delayed profile of  $J_p^G$ .

Table 1 elaborates all the significant parameters related to the 167 geomagnetic storms. By scrutinizing it, we find that the correlation coefficient between the shifted  $J_s^W$  and the  $J_p^G$  indices for 20 events (12% of the total) does not meet the criterion that the significance level (i.e., the  $p$ -value) should be no more than 0.05. Further inspection of these storms reveals that for most of them,  $J_s^W$  is substantially affected by the fluctuating  $B_z$  component in the shaded region, which leads to a poor correlation between the two indices that does not pass the significance test. Besides, the duration of the shaded region could also impact the significance level of the correlation coefficient, as seen in the event that occurred on 2013 October 2. As a result, after excluding these events, we conduct a further detailed statistical analysis on the remaining 147 events. The average time delay for the selected events is  $2.2 (\pm 1.8)$  hr, which is significant in a statistical sense. It may not be generalizable to the majority of events in this paper, as the discrepancy in the time delay among events could be associated with different solar wind structures.

Figure 3 presents a comparison of the correlation coefficients between the initial  $J_s^W$  and the  $J_p^G$  indices and those between the shifted  $J_s^W$  and the  $J_p^G$  indices for 147 geomagnetic storms. There is no clear, uniform relationship between the initial  $J_s^W$  and the  $J_p^G$  indices due to the inconsistent signs of the correlation coefficients for these events. The absolute value of the correlation coefficient for  $\sim 78\%$  of the events does not exceed 0.50, which implies that the two indices are poorly or barely correlated with each other. In contrast, we see a stabilized relationship between the shifted  $J_s^W$  and the  $J_p^G$  indices with a negative correlation coefficient for each event.

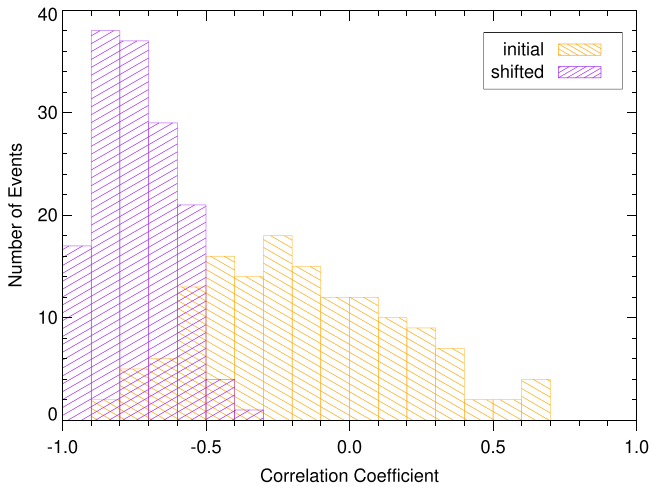


**Figure 3.** Histogram of the correlation coefficients between the initial  $J_s^W$  and  $J_p^G$  indices (orange), as well as those between the shifted  $J_s^W$  and  $J_p^G$  indices (purple) for 147 geomagnetic storms.

This demonstrates the critical importance of the time delay when establishing connections between indices in different regions and the feasibility of the cross-correlation analysis. Given that the correlation coefficient for  $\sim 85\%$  of the events is less than or equal to  $-0.60$ , we suggest that the shifted  $J_s^W$  and the  $J_p^G$  indices are sufficiently anticorrelated with each other. This is consistent with the fact that geomagnetic activity can be considerably affected by the solar wind energy entering the magnetosphere.

For individual events, a linear fit is applied to quantify the relationship between the shifted  $J_s^W$  and the  $J_p^G$  indices, and the resulting parameters ( $k$  and  $b$ ) differ from case to case (see Table 1), which manifests that the disturbance level of the geomagnetic field is subjected to upstream solar wind conditions. In order to acquire a general quantitative profile of the two indices, a statistical analysis is carried out for 147 geomagnetic storms. Figure 4 displays  $J_p^G$  versus the shifted  $J_s^W$  index for all the events. It appears that the two indices do not exhibit a strictly linear relationship, even though the correlation coefficient is approximately  $-0.69$ . Gonzalez & Tsurutani (1987) suggest that a large, negative, and long-duration southward magnetic field component below  $-10$  nT is a key factor in causing intense geomagnetic storms with the minimum  $D_{st}$  index less than  $-100$  nT. In this work, we utilize a  $B_z$  value of  $-10$  nT as a benchmark to perform separate analyses of the correlation between the two indices. Note that the  $B_z$  component in the shaded region for all the events has been synchronized with the shifted  $J_s^W$  index through a backward shift by the same time delay as that of  $J_s^W$ .

As shown in Figure 4, a general trend is clearly observable in which smaller southward magnetic field components correspond to lower values of the shifted  $J_s^W$  index and higher magnitudes of  $J_p^G$ , and the opposite is also true for larger ones. This implies that enhanced southward magnetic field components are closely associated with the injection of increased solar wind energy into the magnetosphere and the occurrence of stronger geomagnetic storms. There are also several data points that deviate from the overall trend, and these outliers are almost unrelated to events with a time delay of more than 5 hr (see Table 1) but are related to severe storms with a minimum  $D_{st}$  value below  $-300$  nT. To ensure the completeness of the statistical analysis, these storms are not

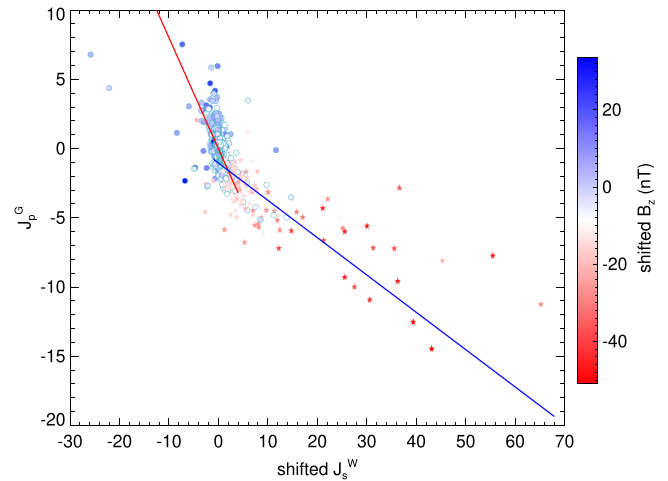


**Figure 4.** Correlation between the shifted  $J_s^W$  and  $J_p^G$  indices for 147 geomagnetic storms. The circles denote indices with  $B_z \geq -10$  nT, and the stars present those with  $B_z < -10$  nT. The lines indicate the results of a robust linear fit of each categorized pair. The color bar shows the magnitude of the shifted  $B_z$  component.

excluded from the present work. We notice that when the  $B_z$  component is greater than or equal to  $-10$  nT, the values of the shifted  $J_s^W$  index are roughly distributed around 0 with a span of 3 from both ends, and most of the  $J_p^G$  values are relatively larger (no less than  $-4$ ) and some are positive. This supports the idea that weaker geomagnetic field perturbations are caused by a reduced level of solar wind energy. We apply a robust outlier-resistant linear fit—a model that can reduce the effects of outliers—to quantify the relationship, which gives  $J_p^G(t) = -0.80 \times J_s^W(t - 2) - 0.01$ . For the remaining data points, the magnitudes of the shifted  $J_s^W$  index are predominantly positive, while those of  $J_p^G$  are largely negative. Many overlaps can also be seen at a  $B_z$  component of around  $-10$  nT. The correlation coefficient between them is  $-0.81$ , and the robust linear fit yields the relationship  $J_p^G(t) = -0.27 \times J_s^W(t - 2) - 1.05$ . These relations presented in Figure 4 suggest that the time series of  $J_p^G$  can be characterized about 2 hr in advance by using  $J_s^W$ , indicating the availability of  $J_s^W$  for providing early warnings of possible geomagnetic field disturbances, which is important for space weather forecasting. In addition, it is noteworthy that all data points do inflect at the  $B_z$  component of  $-10$  nT, and the slope  $k$  for each pair differs significantly. The reasons for this phenomenon are not yet clear and could be studied in future work.

## 5. Conclusions and Discussion

We establish an interplanetary disturbance index ( $J_s^W$ ) from the point of view of energy for the first time by combining the SWM and a solar wind–magnetosphere energy coupling function (the  $\varepsilon$  parameter). It parallels the ionospheric and geomagnetic disturbance indices proposed in previous studies (Chen et al. 2014; Zhao et al. 2022,  $J_p$  and  $J_p^G$ , both are formed based on the same method), and is crucial for achieving quantitative predictions of geomagnetic field variations. This work evaluates how  $J_s^W$  is employed to characterize the evolution of  $J_p^G$ , and a statistical analysis is also performed to

acquire an overall profile of the relationship between the two indices. The results are summarized and discussed below.

Event analyses have revealed that a sudden increase in the  $J_s^W$  index is commonly followed by a delayed reinforcement in the  $J_p^G$  index, verifying the utility of  $J_s^W$  as an indicator of near-Earth solar wind disturbances. The time delay determined from a cross-correlation analysis of the two indices is clearly visible in the majority of events, and it may be the response time of the geomagnetic activity to the injected solar wind energy. This is consistent with the result of Zhao et al. (2022) that the variations of  $J_p^G$  can respond well to the process of injecting solar wind energy with a certain time delay. In their paper, the ring current injection term ( $Q$ ) has been adopted as a proxy of energy. The backward time-shifted  $J_s^W$  and the  $J_p^G$  indices are explicitly anticorrelated with each other, and the deduced  $J_p^G$  index from a linear fit of the two indices is quite analogous to the initial one, which manifests that the energy is indeed an effective proxy linking perturbations in the near-Earth solar wind and the geomagnetic field as required by the internal magnetospheric dynamics. Additionally, the discrepancy in the time delay among events may be attributed to various geo-effective solar wind structures, such as ICMEs, CIRs, high-speed streams, and others (Telloni et al. 2020), i.e., it may be modulated by the mechanism of energy transfer from the near-Earth solar wind to the magnetosphere.

Our work filters out 147 geomagnetic storms by taking the significance level of the correlation coefficient between the shifted  $J_s^W$  and the  $J_p^G$  indices not exceeding 0.05 as a baseline. A statistical analysis of the two indices of these events implies that larger southward magnetic fields are closely related to higher values of  $J_s^W$  as well as smaller magnitudes of  $J_p^G$ . This is consistent with the widely accepted concept of the effect of southward directed IMF on the energy transfer. The two quantitative relationships obtained from a robust linear fit of the two indices suggest that  $J_s^W$  can be utilized to estimate the outline of  $J_p^G$  that is delayed about 2 hr. It is worth noting that this paper evaluates the association between the shifted  $J_s^W$  and the  $J_p^G$  indices for the first time, both of which are dimensionless and constructed using the SWM. This is different from the association of the  $J_p$  and  $D_{st}$  indices given by Chen et al. (2014), as the  $D_{st}$  index is measured with a specific unit. These relations in the present work provide a useful means to predict possible geomagnetic field perturbations based on the same set of indices, which is crucial for space weather monitoring and operational forecasting.

The average time delay between  $J_s^W$  and  $J_p^G$  for 147 geomagnetic storms is about  $2.2 (\pm 1.8)$  hr, which may reflect the intricate process from the injection of upstream solar wind energy to the magnetospheric response to it. As far as we know, the merging of the interplanetary southward magnetic field component with the dayside geomagnetic field would sweep magnetic flux to the Earth's nightside magnetosphere (Dungey 1961). Thereafter, under the impact of the large-scale convective electric fields, the energetic ions and electrons from the near-Earth plasma sheet are injected into the inner magnetosphere, leading to an enhanced westward ring current. This, in turn, can cause a reduction in the horizontal component of the geomagnetic fields, as manifested by a decrease in the  $D_{st}$  index (e.g., Daglis et al. 1999; Daglis 2001). According to Kozyra & Liemohn (2003), the time delay between peak values of the energy input into the ring current and the corrected  $D_{st}$  index can be attributed to the process of ion convection into the

inner magnetosphere, which typically takes a few hours. In this study, the average time delay during the transmission of solar wind energy from the magnetopause to the inner magnetosphere ( $2.2 \pm 1.8$  hr) is consistent with the suggestion of Kozyra & Liemohn (2003). Our result is also acceptable when compared to the time delay between the  $\varepsilon$  parameter and the evolution of the ring current given by Gonzalez et al. (1989) for six intense geomagnetic storms ( $D_{st} < -100$  nT), which is about  $56 (\pm 43)$  minutes.

Finally, our work highlights the geo-effectiveness of enhanced southward magnetic fields in causing geomagnetic storms. The IMF's southward components are often detected in the sheaths, ICMEs, CIRs, and other solar wind structures (e.g., Gosling et al. 1990, 1991; Tsurutani & Gonzalez 1997; Richardson et al. 2006; Zhang et al. 2007; Liu et al. 2014, 2017, 2018, 2020; Hu et al. 2016; Kilpua et al. 2017; He et al. 2018; Chen et al. 2019; Zhao et al. 2019). Nevertheless, the current work puts emphasis on the correlation and time delay between  $J_s^W$  and  $J_p^G$  through individual and statistical analyses. Tracing of the interplanetary source associated with each storm is beyond the scope of this paper and will be discussed in a subsequent work to explore the correlation between the two indices for different solar wind structures. Note that  $J_s^W$  is a preliminary interplanetary disturbance index established by combining the SWM and the empirical  $\varepsilon$  parameter. In future studies, we intend to optimize  $J_s^W$  by analyzing other quantitative energy coupling functions (e.g., Newell et al. 2007; Tenfjord & Østgaard 2013; Wang et al. 2014a), and eventually select the most suitable one to provide early warnings of geomagnetic field perturbations. Furthermore, we will evaluate the correlation between  $J_p^G$  and  $J_p$  to facilitate the application of the novel set of indices constructed from the SWM for the quantitative prediction of the chain impacts caused by transient flows on the solar wind–magnetosphere–ionosphere system.

## Acknowledgments

This research was supported by NSFC under grants 42204176, 42274217, 42274201, 42004145, and 12073032, National Key R&D Program of China (No.2021YFA0718600), China Meteorological Administration “Space Weather Monitoring and Alerting” Key Innovation Team (CMA2024ZD01) and “Ionospheric Forecast and Alerting” Youth Innovation Team (CMA2024QN09), the Strategic Priority Research Program of the Chinese Academy of Sciences (No.XDB0560000), and the Specialized Research Fund for State Key Laboratories of China. We also acknowledge the use of solar wind data from the OMNI database, the geomagnetic field data from INTERMAGNET, and the  $D_{st}$  index from WDC in Kyoto, which are available at [https://spdf.gsfc.nasa.gov/pub/data/omni/low\\_res\\_omni/](https://spdf.gsfc.nasa.gov/pub/data/omni/low_res_omni/), <https://www.intermagnet.org/>, and <https://wdc.kugi.kyoto-u.ac.jp/dstae/index.html>, respectively.

## ORCID iDs

Xiaowei Zhao  <https://orcid.org/0000-0002-4016-5710>  
 Jingsong Wang  <https://orcid.org/0000-0003-2943-6812>  
 Mingxian Zhao  <https://orcid.org/0000-0002-1031-018X>  
 Ying D. Liu  <https://orcid.org/0000-0002-3483-5909>  
 Huidong Hu  <https://orcid.org/0000-0001-8188-9013>  
 Mingzhe Liu  <https://orcid.org/0000-0003-2981-0544>  
 Tian Mao  <https://orcid.org/0000-0001-7340-811X>  
 Qiugang Zong  <https://orcid.org/0000-0002-6414-3794>

## References

- Akasofu, S. I. 1980, *P&SS*, **28**, 495  
 Akasofu, S. I. 1981a, *SSRv*, **28**, 121  
 Akasofu, S. I. 1981b, *P&SS*, **29**, 1151  
 Andriyas, T., & Andriyas, S. 2017, *Ap&SS*, **362**, 160  
 Baker, D. N., Hones, E. W. J., Payne, J. B., & Feldman, W. C. 1981, *GeoRL*, **8**, 179  
 Boroyev, R. N., Vasiliev, M. S., & Baishev, D. G. 2020, *JASTP*, **204**, 105290  
 Boteler, D. H., Pirjola, R. J., & Nevanlinna, H. 1998, *AdSpR*, **22**, 17  
 Chen, C., Liu, Y. D., Wang, R., et al. 2019, *ApJ*, **884**, 90  
 Chen, Z., Wang, J.-S., Deng, Y., & Huang, C.-M. 2017, *JGRA*, **122**, 3632  
 Chen, Z., Wang, J.-S., Huang, C.-M., & Huang, L.-F. 2014, *JGRA*, **119**, 156  
 Cliver, E. W., Boriakoff, V., & Bounar, K. H. 1996, *JGRA*, **101**, 27091  
 Daglis, I. A. 2001, *SSRv*, **98**, 343  
 Daglis, I. A., Thorne, R. M., Baumjohann, W., & Orsini, S. 1999, *RvGeo*, **37**, 407  
 Dungey, J. W. 1961, *PhRvL*, **6**, 47  
 Echer, E., Gonzalez, W. D., Gonzalez, A. L. C., et al. 2004, *JASTP*, **66**, 1019  
 Gonzalez, W. D. 1990, *P&SS*, **38**, 627  
 Gonzalez, W. D., & Echer, E. 2005, *GeoRL*, **32**, L18103  
 Gonzalez, W. D., Joselyn, J. A., Kamide, Y., et al. 1994, *JGR*, **99**, 5771  
 Gonzalez, W. D., & Tsurutani, B. T. 1987, *P&SS*, **35**, 1101  
 Gonzalez, W. D., Tsurutani, B. T., & Clúa de Gonzalez, A. L. 1999, *SSRv*, **88**, 529  
 Gonzalez, W. D., Tsurutani, B. T., Gonzalez, A. L. C., et al. 1989, *JGR*, **94**, 8835  
 Gopalswamy, N., Yashiro, S., Michalek, G., et al. 2005, *GeoRL*, **32**, L12S09  
 Gosling, J. T., Bame, S. J., McComas, D. J., & Phillips, J. L. 1990, *GeoRL*, **17**, 901  
 Gosling, J. T., McComas, D. J., Phillips, J. L., & Bame, S. J. 1991, *JGR*, **96**, 7831  
 Guo, J., Feng, X., Emery, B. A., et al. 2011, *JGRA*, **116**, A051006  
 Hajra, R., Marques de Souza Franco, A., Echer, E., & Bolzan, M. J. A. 2021, *JGRA*, **126**, e28695  
 Hathaway, D. H. 2015, *LRSP*, **12**, 4  
 He, W., Liu, Y. D., Hu, H., Wang, R., & Zhao, X. 2018, *ApJ*, **860**, 78  
 Hu, H., Liu, Y. D., Wang, R., Möstl, C., & Yang, Z. 2016, *ApJ*, **829**, 97  
 Jakowski, N., Stankov, S. M., Schlueter, S., & Klaehn, D. 2006, *AdSpR*, **38**, 2596  
 Jian, L., Russell, C. T., Luhmann, J. G., & Skoug, R. M. 2006, *SoPh*, **239**, 337  
 Kamide, Y. 1992, *JGG*, **44**, 109  
 Kamide, Y., Yokoyama, N., Gonzalez, W., et al. 1998, *JGR*, **103**, 6917  
 Kan, J. R., & Lee, L. C. 1979, *GeoRL*, **6**, 577  
 Katsavrias, C., Preka-Papadema, P., & Moussas, X. 2012, *SoPh*, **280**, 623  
 Kilpua, E., Koskinen, H. E. J., & Pulkkinen, T. I. 2017, *LRSP*, **14**, 5  
 Kishcha, P. V., Dmitrieva, I. V., & Obridko, V. N. 1999, *JASTP*, **61**, 799  
 Koskinen, H. E. J., & Tanskanen, E. I. 2002, *JGRA*, **107**, 1415  
 Kozyra, J. U., & Liemohn, M. W. 2003, *SSRv*, **109**, 105  
 Li, H., Wang, C., Xu, W. Y., & Kan, J. R. 2012, *JGRA*, **117**, A04225  
 Liu, M., Liu, Y. D., Yang, Z., Wilson, L. B., & Hu, H. I. 2018, *ApJL*, **859**, L4  
 Liu, Y. D., Chen, C., & Zhao, X. 2020, *ApJL*, **897**, L11  
 Liu, Y. D., Yang, Z., Wang, R., et al. 2014, *ApJL*, **793**, L41  
 Liu, Y. D., Zhao, X., & Zhu, B. 2017, *ApJ*, **849**, 112  
 Lu, G., Baker, D. N., McPherron, R. L., et al. 1998, *JGR*, **103**, 11685  
 Maggiolo, R., Hamrin, M., De Keyser, J., et al. 2017, *JGRA*, **122**, 109  
 Marques de Souza, A., Echer, E., Bolzan, M. J. A., & Hajra, R. 2018, *AnGeo*, **36**, 205  
 Marques de Souza Franco, A., Hajra, R., Echer, E., & Bolzan, M. J. A. 2021, *AnGeo*, **39**, 929  
 Mayaud, P. N. 1980, *GMS*, **22**, 607  
 McPherron, R. L., Hsu, T.-S., & Chu, X. 2015, *JGRA*, **120**, 2494  
 Meng, C. I., Tsurutani, B., Kawasaki, K., & Akasofu, S. I. 1973, *JGR*, **78**, 617  
 Mursula, K., & Zieger, B. 1996, *JGR*, **101**, 27077  
 Newell, P. T., Sotirelis, T., Liou, K., Meng, C. I., & Rich, F. J. 2007, *JGRA*, **112**, A01206  
 Østgaard, N., Vondrak, R. R., Gjerloev, J. W., & Germany, G. 2002, *JGRA*, **107**, 1246  
 Oughton, E. J., Skelton, A., Horne, R. B., Thomson, A. W. P., & Gaunt, C. T. 2017, *SpWea*, **15**, 65  
 Perreault, P., & Akasofu, S. I. 1978, *GeoJ*, **54**, 547  
 Pirjola, R., Viljanen, A., Pulkkinen, A., & Amm, O. 2000, *PCEC*, **25**, 333  
 Prabhakaran Nayar, S. R., Radhika, V. N., Revathy, K., & Ramadas, V. 2002, *SoPh*, **208**, 359  
 Press, W. H., Teukolsky, S. A., Vetterling, W. T., & Flannery, B. P. 1992, *Numerical Recipes in C: The Art of Scientific Computing* (2nd ed.; Cambridge: Cambridge Univ. Press)  
 Pulkkinen, T. I., Ganushkina, N. Y., Kallio, E. I., et al. 2002, *AdSpR*, **30**, 2231  
 Richardson, I. G., Webb, D. F., Zhang, J., et al. 2006, *JGRA*, **111**, A07S09  
 Riley, P., Baker, D., Liu, Y. D., et al. 2018, *SSRv*, **214**, 21  
 Rostoker, G. 1972, *RvGSP*, **10**, 935  
 Tapping, K. F. 2013, *SpWea*, **11**, 394  
 Telloni, D., Carbone, F., Antonucci, E., et al. 2020, *ApJ*, **896**, 149  
 Tenfjord, P., & Østgaard, N. 2013, *JGRA*, **118**, 5659  
 Tsurutani, B. T., & Gonzalez, W. D. 1997, *GMS*, **98**, 77  
 Turner, N. E., Cramer, W. D., Earles, S. K., & Emery, B. A. 2009, *JASTP*, **71**, 1023  
 Usoskin, I. G. 2017, *LRSP*, **14**, 3  
 Vasyliunas, V. M., Kan, J. R., Siscoe, G. L., & Akasofu, S. I. 1982, *P&SS*, **30**, 359  
 Verbanac, G., Vršnak, B., Temmer, M., Manda, M., & Korte, M. 2010, *JASTP*, **72**, 607  
 Verbanac, G., Vršnak, B., Veronig, A., & Temmer, M. 2011, *A&A*, **526**, A20  
 Vichare, G., Alex, S., & Lakhina, G. S. 2005, *JGRA*, **110**, A03204  
 Wang, C., Han, J. P., Li, H., Peng, Z., & Richardson, J. D. 2014a, *JGRA*, **119**, 6199  
 Wang, J. S., Chen, Z., & Huang, C. M. 2014b, *AnGeo*, **32**, 563  
 Zhang, J., Richardson, I. G., & Webb, D. F. 2008a, *JGRA*, **113**, A00A12  
 Zhang, J., Richardson, I. G., Webb, D. F., et al. 2007, *JGRA*, **112**, A10102  
 Zhang, Y., Sun, W., Feng, X. S., et al. 2008b, *JGRA*, **113**, A08106  
 Zhao, M.-X., Wang, J.-S., & Zhao, X.-W. 2022, *Univ*, **8**, 506  
 Zhao, X., Liu, Y. D., Hu, H., & Wang, R. 2019, *ApJ*, **882**, 122